Journal of Materials Chemistry B

Multi-responsive Hydrogels Derived from the Self-assembly of Tethered Allyl-functionalized Racemic Oligopeptides

Journal:	*Journal of Materials Chemistry B*
Manuscript ID:	TB-ART-06-2014-000909.R1
Article Type:	Paper
Date Submitted by the Author:	04-Jul-2014
Complete List of Authors:	He, Xun; Texas A&M University, Fan, Jingwei; Texas A&M University, Chemistry Zhang, Fuwu; Texas A&M University, Chemistry Li, Richen; Texas A&M University, Chemistry Pollack, Kevin; Texas A&M University, Raymond, Jeffery; Texas A&M University, Laboratory for Synthetic-Biologic Interactions; Texas A&M University, Chemistry Zou, Jiong; Texas A&M University, Wooley, Karen; Texas A&M University, Chemistry

Cite this: DOI: 10.1039/c0xx00000x

www.rsc.org/xxxxxx

ARTICLE TYPE

Multi-responsive Hydrogels Derived from the Self-assembly of Tethered Allyl-functionalized Racemic Oligopeptides

Xun He, Jingwei Fan, Fuwu Zhang, Richen Li, Kevin A. Pollack, Jeffery E. Raymond, Jiong Zou,* and Karen L. Wooley*

Received (in XXX, XXX) Xth XXXXXXXXX 20XX, Accepted Xth XXXXXXXXX 20XX
DOI: 10.1039/b000000x

A multi-responsive triblock hydrogelator oligo(DL-allylglycine)-*block*-poly(ethylene glycol)-*block*-oligo(DL-allylglycine) (ODLAG-*b*-PEG-*b*-ODLAG) was synthesized facilely by ring-opening polymerization (ROP) of DLAG *N*-carboxyanhydride (NCA) with a diamino-terminated PEG as the macroinitiator. This system exhibited heat-induced sol-to-gel transitions and either sonication- or enzyme-induced gel-to-sol transitions. The *β*-sheeting of the oligopeptide segments was confirmed by attenuated total reflection Fourier transform infrared spectroscopy (ATR-FTIR) and wide-angle X-ray scattering (WAXS). The *β*-sheets further displayed tertiary ordering into fibrillar structures that, in turn generated a porous and interconnected hydrogel matrix, as observed *via* transmission electron microscopy (TEM) and scanning electron microscopy (SEM). The reversible macroscopic sol-to-gel transitions triggered by heat and gel-to-sol transitions triggered by sonication were correlated with the transformation of nanostructural morphologies, with fibrillar structures observed in gel and spherical aggregates in sol, respectively. The enzymatic breakdown of the hydrogels was also investigated. This allyl-functionalized hydrogelator can serve as a platform for the design of smart hydrogels, appropriate for expansion into biological systems as bio-functional and bio-responsive materials.

Introduction

Stimuli-responsive hydrogels have attracted significant attention in the last two decades with a wide range of applications being targeted for controlled drug release,[1] tissue engineering,[2] flow control,[3] and selective sensing[4]. Commonly used stimuli for responsive hydrogels include temperature[5, 6], light,[7] pH,[8] enzymes,[9] sonication,[10] and oxidation-reduction.[11] Temperature, pH, and enzymes are particularly interesting stimuli for applications in biological systems. In part, this is due to local physiological environments being different from *ex situ* environments, which can lead to highly specific triggered response for systems that need both sol and gel type behaviour during different periods of their usage. Applied stimuli typically trigger construction or deconstruction of the hydrogel networks by either covalent[12] or non-covalent interactions.[5] Recently, hydrogels composed of materials with non-covalent interactions have received attention due to their ability to rapidly respond to physical or chemical stimuli, the versatility to self assemble into different nano- or micro-structures in different environments, and the ability to exhibit changes in macroscopic characteristics, such as sol-gel transitions.[13, 14] Compared with single stimulus-responsive systems, dual- or multi-responsive hydrogels provide higher flexibility in material fabrication and opportunities to achieve greater control of physical configurations or additional kinetic properties (*e.g.* degradation or drug release).[15, 16] For instance, Lee *et al.* reported an injectable hydrogel, for which hydrogelation occurred with a slight change of the pH at physiological conditions upon injection, followed by slow release of insulin owing to the hydrolytic degradation of polymer backbone.[17] A difficulty in developing a catalogue of multi-responsive systems is the requirement for precise control of one or more chemistries within the system, ultimately, leading to increasingly difficult synthetic approaches. The generation of multi-responsive materials, thus, remains a challenge.

The generation of peptide-based hydrogels is a topic of intense interest to achieve increased biocompatibility,[18, 19] specific enzymatic response[20, 21] and versatility of supramolecular assembly.[22] The formation of these hydrogel matrices can be attributed, in the majority of cases, to the entanglement of fibrillar structures assembled through noncovalent interactions, such as hydrogen bonding,[23] *π*-*π* stacking,[24] electrostatic interactions,[25] and/or hydrophobic interactions.[26, 27] A focus on hydrogen bonding in peptide-rich systems is particularly appropriate, as it is a primary factor in the formation of robust secondary structures, including *α*-helix[28-30] or *β*-sheet,[25] depending on the type or sequence of amino acids. Specifically, we are interested in the

utilization of DL-allylglycine. The ease with which various functionalities can be incorporated into poly(DL-allylglycine) (PDLAG) through thiol-ene click chemistry[31] and the strong gelation properties it possesses in organic solvents[32] make it an ideal candidate for advanced applications when compared with other *β*-sheet-forming peptides composed of natural amino acids (*e.g.* valine, alanine, isoleucine, *etc.*). Recently, gels composed of PEG-*b*-*β*-sheet-peptides synthesized by ring-opening polymerization (ROP) of *N*-carboxyanhydrides (NCAs) have been described by Jeong,[33] Heise,[34] Li,[35] and Chen[36] to show a reverse thermal gelation profile (heat-induced sol-to-gel transition), and have been reported by our group to exhibit gel-to-sol or gel-to-gel behavior with sonication.[37] To the best of our knowledge, oligo or polyDLAG have not been used directly in the formation of hydrogels. Therefore, we chose to investigate this system to determine its stimuli-responsive properties by seeking a suitable chemical structure and hydrophobic-hydrophilic balance.

Herein, we report a thermo-, sonication-, and enzyme-responsive ODLAG-*b*-PEG-*b*-ODLAG hydrogelator. The hydrophobic blocks are synthesized facilely by ring-opening polymerization of racemic allylglycine. Although racemic peptides (*vs.* stereo-regular peptides) are reported to have a lower ability to form *α*-helix or *β*-sheet secondary structures,[28, 38, 39] these ODLAG-*b*-PEG-*b*-ODLAG hydrogels were found to have critical gelation concentrations as low as 1.0 wt%. Furthermore, in contrast to many polypeptide-based hydrogelators which undergo gel melting with increased temperature,[26, 40] a reverse thermal gelation profile was observed. The driving force for this heat induced gelation is discussed in conjunction with a comprehensive study of the responsive behaviors. This multi-responsive hydrogel system is appropriate to serve as a platform for the development of drug delivery vehicles, sensors, and smart devices.

Experimental

Materials

Ethyl acetate, *n*-hexane, tetrahydrofuran (THF), diethyl ether, *N,N*-dimethylformamide (DMF, anhydrous, ≥ 99.8%), trifluoroacetic acid (TFA), DL-allylglycine, *α*-pinene, and triphosgene were purchased from Sigma-Aldrich Company (USA). *α,ω*-Diamino-terminated poly(ethylene glycol) (NH_2-PEG_{68}-NH_2, M_n = 3000 g/mol) was purchased from Rapp Polymere (Germany). All chemicals were used without further purification, unless otherwise noted. Nanopure water (18 MΩ·cm) was acquired by means of a Milli-Q water filtration system, Millipore Corp (USA).

Instrumentation

^{1}H and ^{13}C NMR spectra were recorded on a Varian Inova 300 spectrometer interfaced to a UNIX computer using VnmrJ software. Chemical shifts were referenced to the solvent resonance signals. Attenuated total reflection Fourier transform infrared spectroscopy (ATR-FTIR) spectra were recorded on an IR Prestige 21 system (Shimadzu Corp.) and analyzed using IRsolution v. 1.40 software.

Matrix assisted laser desorption ionization mass spectrometry (MALDI-TOF MS) was performed on a Kratos/Shimadzu Axima CFR (Manchester, England) MALDI-TOF mass spectrometer. Ions were generated by nitrogen laser at 337 nm, a frequency of 10 Hz, and an acceleration voltage of 25 kV. Dithranol was used as the matrix. The polymer sample was dissolved in TFA (10 mg/mL), and dithranol was dissolved in THF (35 mg/mL). The sample solution was mixed with the matrix at a volume ratio of 1:1 before being spotted onto a sample plate. The sample was then analyzed under linear conditions.

Thermogravimetric analysis (TGA) was performed under argon atmosphere using a Mettler Toledo model TGA/DSC 1 (Mettler Toledo, Inc., Columbus, OH), with a heating rate of 10 °C/min. Measurements were analyzed using Mettler Toledo STAR^e v. 7.01 software. Glass transition temperatures (T_g) were measured by differential scanning calorimetry (DSC) on a Mettler Toledo DSC822®, with a heating rate of 10 °C/min and a cooling rate of 10 °C/min. Measurements were analyzed using Mettler Toledo STAR^e v. 7.01 software. The T_g was taken as the midpoint of the inflection tangent, upon the third heating scan.

Wide-angle X-ray scattering (WAXS) was performed on a Bruker D8 Bragg-Brentano X-ray powder diffractometer. The sample was placed in the sample holder of a two circle goniometer, enclosed in a radiation safety enclosure. The X-ray source was a 2.2 kW Cu X-ray tube, maintained at an operating current of 40 kV and 40 mA. The X-ray optics was the standard Bragg-Brentano para-focusing mode with the X-ray diverging from a DS slit (1 mm) at the tube to strike the sample and then converging at a position sensitive X-ray Detector (Lynx-Eye, Bruker-AXS). The two-circle 250 mm diameter goniometer was computer controlled with independent stepper motors and optical encoders for the θ and 2θ circles with the smallest angular step size of 0.0001° 2θ. The software suit for data collection and evaluation was window based. Data collection was automated COMMANDER program by employing a DQL file and analyzed by the program EVA.

Dynamic mechanical analysis (DMA) was performed on a Mettler Toledo TT-DMA system. DMA measurements of the hydrogels (5 wt%) were performed over 3 h in compression on a 3.2 mm thick, 10 mm diameter cylinder. Dynamic measurements were recorded over a range of 0.1 to 10 Hz at room temperature with static stress modulated to 2% compression and a dynamic force applied to provide ± 1% deformation. Kinetic data presented were obtained as a single exponential decay using Origin Pro 8.1 software.

Transmission electron microscopy (TEM) images were collected on a JEOL 1200 EX operating at 100 kV and micrographs were recorded at calibrated magnifications using a SLA-15C CCD camera. Samples for TEM measurements were prepared as follows: 10 μL of the dilute solution was deposited onto a carbon-coated copper grid, and after 2 min, the excess of the solution was quickly wicked away by a piece of filter paper. The samples were then negatively stained with 1 wt% phosphotungstic acid (PTA) aqueous solution. After 30 s, the excess staining solution was quickly wicked away by a piece of filter paper and the samples were left to dry under vacuum overnight.

Scanning electron microscopy (SEM) imaging was performed in JOEL JSM-6400 SEM operated at an acceleration voltage of 15 kV. The preparation of samples for SEM involved placing a

drop of hydrogel on a carbon thin film. The gel was then subjected to immediate freezing by liquid nitrogen, followed by lyophilization for 3 days. The surface of the gel was sputter coated with gold for 3 min under argon before imaging.

Sonication was performed in an ultrasonic homogenizer (maximum power, 150 W, 20 kHz, Model 150 V/T, Biologics, Inc.) equipped with a micro tip with a diameter of 3.81 mm, employing the power output of 30 W in the frequency of 20 kHz at room temperature.

Synthesis

Synthesis of DL-allylglycine *N*-carboxyanhydride (DLAG NCA). The DLAG NCA monomer was prepared following the previously reported method.[41] In a 250 mL two-neck flask, equipped with septum and pipet for nitrogen inlet and a condenser with a tubing connector that allowed outlet flow through a base solution ($NaOH_{(aq)}$), DL-allylglycine (2.52 g, 21.9 mmol) was dissolved in 100 mL THF and triphosgene (5.41 g, 18.2 mmol) was added directly to the reaction flask. α-Pinene (7 mL) was then added and the reaction mixture was allowed to stir for 2.5 h at 50 °C, while being constantly flushed with a stream of dry nitrogen. The crude product was concentrated and precipitated from *n*-hexane, recrystallized four times from ethyl acetate/*n*-hexane 1:8 (v/v), and then dried *in vacuo*; yielding 1.02 g (40%) of product as a white needle-like crystal. ^{1}H NMR (300 MHz, $CDCl_3$, ppm): δ 2.55 and 2.75 (m, 2 H, CH_2), 4.42 (m, 1 H, CH), 5.31 (m, 2 H, H_2C=CH), 5.77 (m, 1 H, H_2C=C*H*), 6.55 (br, 1 H, NH). ^{13}C NMR (75 MHz, $CDCl_3$, ppm): δ 36.0, 57.4, 121.7, 130.0, 152.7, 169.0. FT-IR (cm^{-1}): 3345, 3017, 2934, 1825, 1748, 1290, 926. HRMS: calculated $[M-H]^-$ for $C_6H_7NO_3$: 140.0353, found: 140.0354.

Synthesis of ODLAG-*b*-PEG-*b*-ODLAG. A typical procedure for the preparation of ODLAG-*b*-PEG-*b*-ODLAG was as follows: into a flame-dried 25 mL Schlenk flask equipped with a stir bar and capped with a rubber stopper with a needle outlet connected to a tube filled with drying agent, DLAG-NCA (281.9 mg, 1.998 mmol) in DMF (8 mL) was injected. After being stirred at room temperature for 5 min, NH_2-PEG_{68}-NH_2 (497.6 mg, 0.1659 mmol) in DMF (8 mL) was injected *via* a syringe. The reaction mixture was stirred at room temperature (stir rate = 340 rpm) under continuous nitrogen flow (flow rate = 100 mL/min) for 6 h. The reaction mixture was then precipitated into 180 mL diethyl ether twice. The triblock was centrifuged, collected, and dried *in vacuo* to yield 450.0 mg (64.8%) as a white powder. ^{1}H NMR (300 MHz, DMSO-d_6, ppm): δ 2.34 (br, 24 H, $CHCH_2CHCH_2$), 3.50 (br, 272 H, OCH_2) 4.34 (br, 12 H, NHCHCO), 5.00 (br, 24 H, CH_2CHCH_2), 5.69 (br, 12 H, CH_2CHCH_2), 8.09 (br, 12 H, COCHNH). ^{13}C NMR (75 MHz, DMSO-d_6, ppm): δ 36.5, 52.1, 69.8, 117.5, 134.0, 170.5. FT-IR (cm^{-1}): 3672-3402, 3284, 3075, 2870, 1667, 1626, 1526, 1101, 696. DSC: T_g = -18 °C, T_c = 4 °C, T_m = 37 °C, T_g = 102 °C. TGA: 25-303 °C: 0% mass loss, 303-376 °C: 26% mass loss, 376-423 °C: 50% mass loss, 423-500 °C: 3% mass loss, 21% mass remaining above 500 °C. Other copolymers with different degrees of polymerization (DP) were similarly prepared, and the compositions of the resulting copolymers are listed in Table 1.

Results and discussion

With our general interest in the creation of biodegradable stimuli-responsive materials that are synthetically approachable while also being modifiable, specifically for applications in biology and medicine, we began investigations into the syntheses and gelation properties of peptide-containing amphiphilic block copolymers with easily modifiable allyl side chain groups. Recently, our group reported a polypeptide-based organogelator, PEG-*b*-PDLAG, with ultralow critical gelation concentrations (*ca.* 0.1 wt%) in various organic solvents.[32] Here, we took advantage of the strong gelation capability of PEG-*b*-PDLAG system in organic solvents and extended this capability into aqueous medium by designing a triblock structure, in which two oligopeptide segments were tethered by a central PEG block (Scheme 1).

NCA ROPs have been widely used in the syntheses of polypeptide-based materials with well-defined structures at large scales because of the advancement of living polymerization strategies that have occurred in the last two decades.[42-46] Recently, we found that NCA ROPs can be conducted by normal Schlenk techniques, with the enhancement of polymerization rates and retention of living features by a straightforward N_2 flow method.[47] Therefore, in this synthetic route, ROP of DLAG NCA (**M**) with continuous N_2 flow (100 mL/min) over the reaction solution was utilized with α,ω-diamino-terminated poly(ethylene glycol) (NH_2-PEG_{68}-NH_2, **I**) as a macroinitiator. For each polymerization (Table 1), varied ratios of NCA monomer and PEG initiator were dissolved in anhydrous DMF and the ROPs were allowed to proceed for 6 h at room temperature, until the monomer conversions had reached *ca.* 99%, as determined by the intensity of NCA anhydride absorption at 1786 cm^{-1} from attenuated total reflectance-Fourier transform infrared spectroscopy (ATR-FTIR). The reaction mixtures were then precipitated into diethyl ether and dried under vacuum to yield the triblock structures with controlled block sizes as white solids.

The degrees of polymerization and molecular weights were determined by ^{1}H NMR spectroscopy and MALDI-TOF mass spectrometry. Fortuitously, our systems had a delayed gelation response in DMSO, allowing confirmation of polymerization by ^{1}H NMR spectroscopy. In addition, degrees of polymerization were analyzed by comparison of the intensities of methylene proton resonances of the PEG chain at *ca.* 3.5 ppm (f in Fig. 1) with the intensities of ODLAG methine proton at *ca.* 5.7 ppm (d in Fig. 1), or the alkenyl protons at *ca.* 5.0 ppm (e and e' in

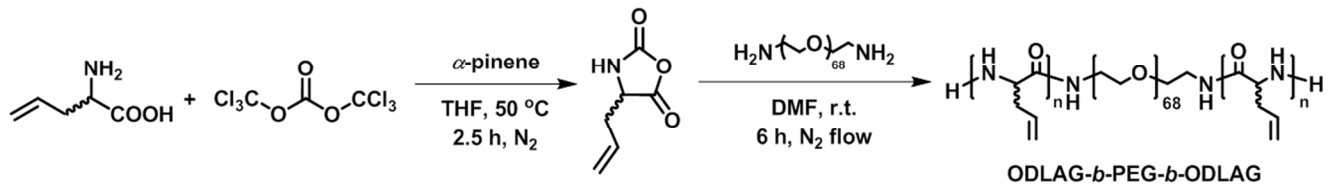

Scheme 1 Synthesis of $ODLAG_6$-*b*-PEG_{68}-*b*-$ODLAG_6$

Table 1 Synthesis and hydrogelation capabilities of ODLAG-*b*-PEG-*b*-ODLAG with different lengths of ODLAG blocks

Polymer	$[\mathbf{I}]_0 : [\mathbf{M}]_0$	DP_n [a]	Hydrogelation [b]	C_{gel} [b,d]
1	1 : 5	5	No	N/A
2	1 : 12	12	Yes	1.0 wt%
3	1 : 18	18	No[c]	N/A

[a] Degree of polymerization, calculated by ^{1}H NMR spectroscopy, equal to the total number of the repeating units of both ODLAG blocks; [b] determined by test tube inversion method; [c] precipitates were observed; [d] critical gelation concentrations, in water

Fig. 1), or the methylene protons at *ca.* 2.3 ppm (c in Fig. 1). A MALDI-TOF measurement using dithranol as matrix was also carried out to characterize the molecular weight of $ODLAG_6$-*b*-PEG_{68}-*b*-$ODLAG_6$. As shown in Fig. S1, the distribution with molecular weight centered at *ca.* 4.0 kDa was consistent with the number-average molecular weight calculated by ^{1}H NMR (*ca.* 4.2 kDa). Due to gelation or aggregate formation in most of the organic solvents (Table S1), gel permeation chromatography (GPC) was not employed to characterize the polymer.

The ability to form hydrogels for ODLAG-*b*-PEG-*b*-ODLAG with different block lengths of oligopeptides was explored (Table 1). It can be concluded from the data of Table 1 that precise control of block lengths for the oligopeptides is required for gelation. Polymers **1** or **3**, which had either shorter or longer block lengths of oligopeptides, compared with polymer **2**, respectively, did not form hydrogels. In addition, polymer **2** was also investigated for its ability to disperse single-walled carbon nanotubes (SWCNTs) in organic solvents.[48]

A thorough assessment of the physical gelation properties of $ODLAG_6$-PEG_{68}-$ODLAG_6$ hydrogels was performed, with data presented in Fig. 2. To prepare the hydrogel systems, denoted weight fractions of polymers and aqueous media were mixed and sol-to-gel transitions were observed when the systems were heated to the gel transition temperatures (T_{gel}), which were measured by the test tube inversion method with a temperature increment step of 1 °C per 20 min. The formed hydrogels were stable and no gel-to-sol transitions were observed when they were left undisturbed for a long period (> 2 weeks) at room temperature. In order to probe the effect of polymer concentration on T_{gel}, the T_{gel} values of a series of hydrogels with varying polymer concentration of **2** were measured. The sol-gel phase diagram revealed that T_{gel} decreased with increase of polymer concentration from 1.0 wt% (95 °C) to 10 wt% (80 °C), and was then maintained at *ca.* 80 °C. Furthermore, DMA was used to assess the mechanical response of the gels. A hydrogel with a polymer concentration of 5 wt% was used in the DMA study, which produced a robust gel appropriate for high frequency operation. With larger operating frequency, both the storage (*E'*) and loss (*E"*) moduli increased at similar rate, indicating a shear thickening response (Fig. S2a). Given the time-temperature superposition principle of DMA, this finding is expected for a gel system with triggered gelation at increased temperatures. During the overall range of frequency modulation (0.1 to 10 Hz), *E*" maintained smaller than *E*', indicating no gel-to-sol transition was taking place in this frequency range at room temperature. In fact, the tan(δ) data indicated increased stiffness with sustained shear as well (Fig. S2b).

In order to study the driving force for the sol-to-gel transition, the supramolecular structure of the dried hydrogel was

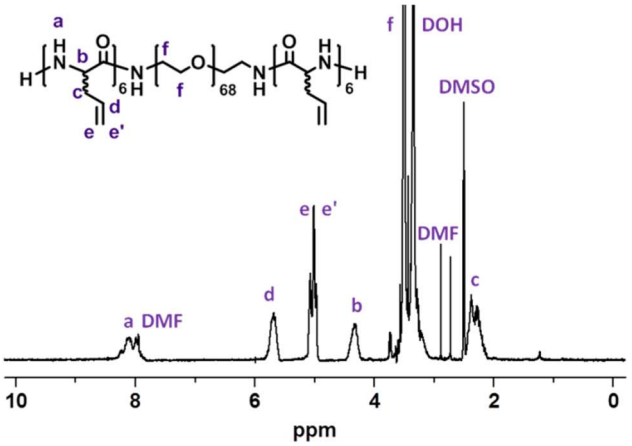

Fig. 1 ^{1}H NMR spectrum of $ODLAG_6$-*b*-PEG_{68}-*b*-$ODLAG_6$.

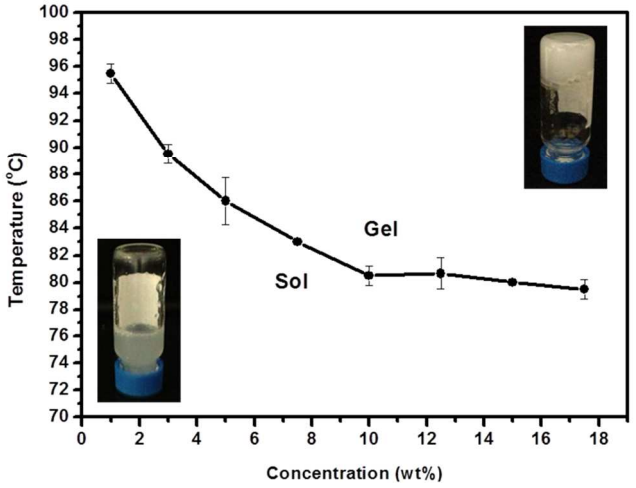

Fig. 2 T_{gel} of $ODLAG_6$-*b*-PEG_{68}-*b*-$ODLAG_6$ hydrogel as a function of polymer concentration.

investigated by ATR-FTIR and WAXS, with both characterization techniques indicating the existence of β-sheet conformations. Characteristic strong absorption of an amide I band at 1626 cm^{-1} and a shoulder peak at 1667 cm^{-1} were attributed to corresponding parallel and antiparallel β-sheet conformations of the peptide blocks, respectively (Fig. 3a).[25, 49] In addition, a peak in the amide II region at 1526 cm^{-1} and an amide V band at *ca.* 700 cm^{-1} were observed in accordance with β-sheet structures, in contrast to peptides with α-helix conformations, which tend to have low or no absorption at *ca.* 700 cm^{-1}.[50, 51] Comparison of ATR-FTIR spectra with NH_2-PEG_{68}-NH_2 and DLAG NCA, which expressed no characteristic peaks in these regions, indicated that the β-sheeting was due to the formation of ODLAG blocks upon polymerization.

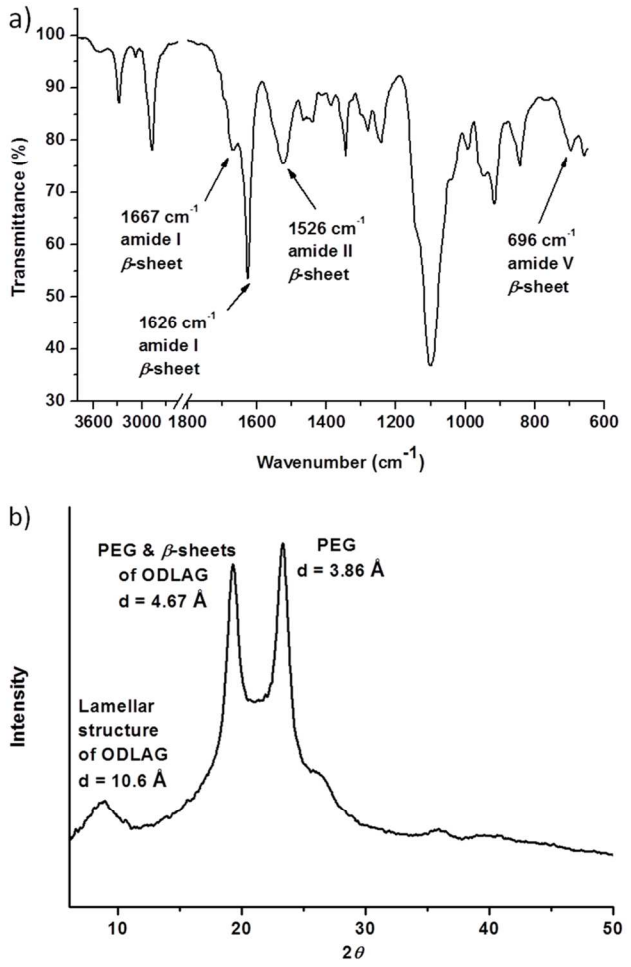

Fig. 3 (a) ATR-FTIR spectrum and (b) WAXS pattern of a dried hydrogel made from ODLAG$_6$-*b*-PEG$_{68}$-*b*-ODLAG$_6$.

WAXS study also confirmed the existence of *β*-sheets. The *d* spacing of 10.6 Å was assigned to the inter-sheet distance of peptide segments (Fig. 3b).[52, 53] A *d* spacing of *ca.* 4.67 Å was described in a variety of *β*-sheet forming peptides as a characteristic hydrogen bonding length in the conformation of *β*-sheet secondary structures.[37, 54, 55] This WAXS signal overlapped with the 120 reflection of monoclinic PEG crystals,[49] which together with the signal corresponding to a d spacing of 3.86 Å correlated well with the crystallization and melting peaks in the DSC trace (Fig. S3).

TEM and SEM were also utilized to characterize the nanostructural morphologies of the ODLAG$_6$-*b*-PEG$_{68}$-*b*-ODLAG$_6$ hydrogel. The TEM sample was prepared with a polymer concentration of 1 mg/mL from dilution of a 5 wt% hydrogel, and stained by a PTA aqueous solution. Fibrillar morphologies with micron scale fibers were observed as bundles in many cases (Fig. 4a and Fig. S4). Reasonable contributions to the formation of bundles include supramolecular cross-linking from residual peptide chain ends at the surface of the fibrils and inter-fibrillar PEG-PEG interactions arising from strong semi-crystalline binding sites. To visualize the ODLAG$_6$-*b*-PEG$_{68}$-*b*-ODLAG$_6$ hydrogel on the microscale, SEM was used on samples that were prepared by freeze-drying (to maintain the network structures of hydrogels). From SEM, it can be observed that three-dimensional interconnected networks were formed in the system, a necessary feature of hydrogels (Fig. 4b). The network possessed a highly porous structure with a broad range of pore sizes (Fig. S5). Direct observation of network porosity is fortunate, as it allows for the potential to encapsulate cargoes such as therapeutic drugs or cells in biological applications.

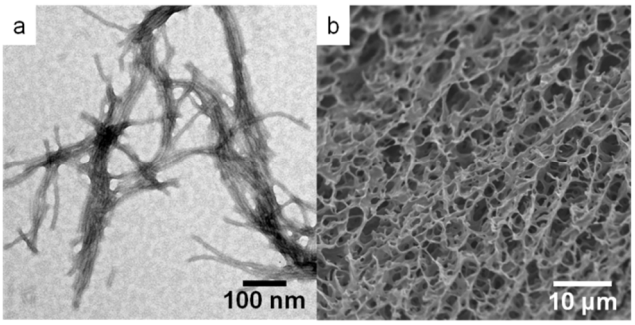

Fig. 4 (a) TEM and (b) SEM images of a ODLAG$_6$-*b*-PEG$_{68}$-*b*-ODLAG$_6$ hydrogel.

Based on the results from ATR-FTIR, WAXS, TEM and SEM analyses, a mechanism for the hydrogelation of ODLAG$_6$-*b*-PEG$_{68}$-*b*-ODLAG$_6$ can be proposed (Scheme 2). Self assembly of the triblock structures into fibers is driven by intermolecular hydrogen bonding of oligopeptide blocks (in red) as hydrophobic domains, which further self-organize into parallel or antiparallel *β*-sheets. The hydrophilic PEG block (in blue) prevents precipitation of the fibers by increasing the aqueous solubility, and maintains the hydrogel structure by capturing water molecules. The thermo-gelation profile may result from heat-induced formation of *β*-sheets and lower water occupancy of the volume that would normally have strong PEG-water associations at lower temperatures, both of which can enhance the hydrophobic interactions.[33-36, 56] As observed in TEM, supramolecularly cross-linked fibers can be formed, with possible mechanisms including inter-fibrillar peptide-peptide interaction or PEG-PEG associations. The entanglement resulting from long range interactions of fibers plays an integral part in the construction of the hydrogel matrix, as observed by SEM.

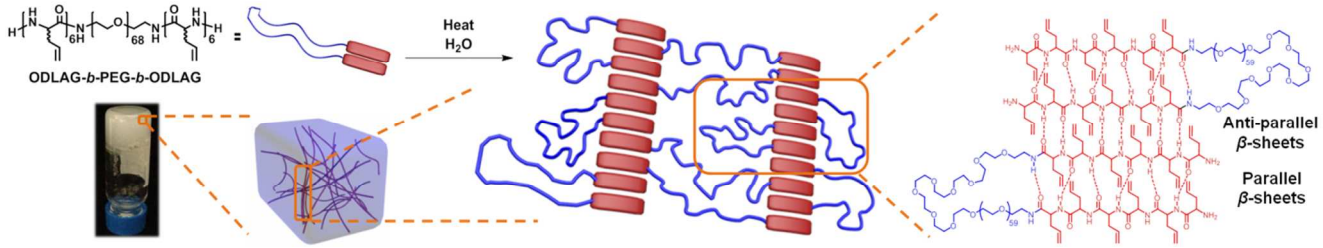

Scheme 2 An illustrative scheme for the formation of nanofibers and hydrogels formed from self-assembly of ODLAG$_6$-*b*-PEG$_{68}$-*b*-ODLAG$_6$.

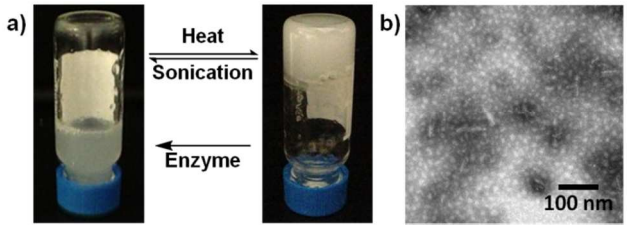

Fig. 5 (a) Digital photographs showing responsiveness of $ODLAG_6$-*b*-PEG_{68}-*b*-$ODLAG_6$ hydrogels towards different stimuli. (b) TEM image of a $ODLAG_6$-*b*-PEG_{68}-*b*-$ODLAG_6$ sol.

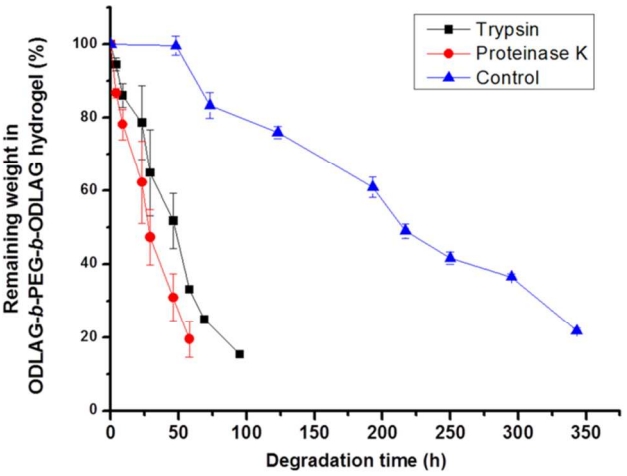

Fig. 6 Weight loss profile of $ODLAG_6$-*b*-PEG_{68}-*b*-$ODLAG_6$ hydrogel with/without enzyme. Measurements were repeated five times for each enzyme and control sample.

The multi-responsive properties of $ODLAG_6$-*b*-PEG_{68}-*b*-$ODLAG_6$ hydrogels (Fig. 5a), and the correlation of nanostructure with physical behaviour were investigated. As shown in the phase diagram (Fig. 2), a reverse thermal gelation behavior was observed. Sol-to-gel transitions occurred by maintaining the sol state at T_{gel} for 20 min, while gel-to-sol transitions were achieved by sonication in less than 10 s. The sol-gel transitions could be conducted for a minimum of 5 cycles without apparent change in gel transition temperatures, which indicated the reversibility of the supramolecular assembly of these physical hydrogels. In order to further understand the hydrogelation and gel breaking behaviors, TEM was employed to compare the differences in nanostructural morphologies between the sol and gel states. The sol state sample was prepared by subjecting the hydrogel to sonication for 10 s, followed by dilution and staining using similar methods to the hydrogel sample. Drastically different from the micrometer-long fibrillar morphologies observed in the gel state (Fig. 4a), spherical aggregates and shorter nanofibrils (*ca.* 100 nm in length) were observed for the sol state (Fig. 5b). The sonication-promoted gel-to-sol transition implies a fundamental disruption of the fibrils, converting them into spherical aggregates incapable of long range interactions, and not a mere disruption of long range fiber interactions.

Enzyme-responsiveness of this hydrogel system was observed by studying *in vitro* hydrogel weight loss profiles, which were assessed by measuring the weight loss of hydrogels (5 wt%) kept at 37 °C in 1.5 mL vials. Tris-HCl buffer (0.05 M, pH = 8.0, 0.2 wt% NaN_3) containing 1 mg/mL proteinase K or trypsin was used as the degradation medium, and hydrogels with Tris-HCl buffer were used as the control. The buffer solution (0.5 mL) was gently added into each vial prior to hydration, and was removed along with any gel debris that had accumulated. According to the weight loss profiles, hydrogels that were subjected to enzymes (proteinase K and trypsin) broke down much faster than did the control (Fig. 6). For example, around 70% and 50% weight losses in 48 h were observed for the hydrogels kept in the medium with proteinase K and trypsin, respectively, while *ca.* 15% weight loss for the control was observed in 72 h. The enzyme accelerated weight loss of the hydrogels may be a result of the surface erosion and the fast degradation of the oligopeptide chains.

Conclusions

In summary, a series of multi-responsive hydrogels composed of PEG tethered oligopeptides, was prepared with extraordinarily low synthetic complexity. The triblock system exhibited reversible and repeatable sol-to-gel and gel-to-sol transitions that can be triggered by heat and sonication, respectively. In addition, certain enzymes accelerated the breakdown of the bio-responsive hydrogels into sols. The ability to form hydrogels is shown to be dependent on the hydrophobic and hydrophilic balance and is dictated by the block length of the oligopeptide blocks, which is in turn easily controlled by reaction feed ratio. Detailed characterization studies indicated that hydrogelation may be driven by a combination of oligopeptide β-sheeting and a balance between PEG-PEG interactions and PEG-water interactions, with effects observed at the supramolecular, nano-, micro- and macro-scales. Moreover, the oligopeptide segments carry reactive allyl side chain groups, which have the potential to be further functionalized into intelligently-designed systems of increased complexity and functionality. This multi-responsive hydrogel system provides a potential platform for development of drug delivery vehicles, sensors, and smart devices.

Acknowledgements

This work was supported in part from the National Heart Lung and Blood Institute of the National Institutes of Health as a Program of Excellence in Nanotechnology (HHSN268201000046C) and the National Science Foundation under grant number DMR-1105304. The Welch Foundation is gratefully acknowledged for support through the W. T. Doherty-Welch Chair in Chemistry (A-0001). The Microscopy & Imaging Center (MIC) at Texas A&M University is also gratefully acknowledged.

Notes and references

*Departments of Chemistry, Chemical Engineering, and Materials Science and Engineering, Laboratory for Synthetic-Biologic Interactions, Texas A&M University, P.O. BOX 30012, 3255 TAMU, College Station, TX 77842, USA. * Corresponding authors: E-mail: jiong.zou@chem.tamu.edu; wooley@chem.tamu.edu; Tel: +1-979-845-4077*

† Electronic Supplementary Information (ESI) available. See DOI: 10.1039/b000000x/

1. M. R. Islam, Y. Gao, X. Li and M. J. Serpe, *J. Mater. Chem. B*, 2014, **2**, 2444.
2. H. Cui, Y. Liu, Y. Cheng, Z. Zhang, P. Zhang, X. Chen and Y. Wei, *Biomacromolecules*, 2014, **15**, 1115.
3. D. J. Beebe, J. S. Moore, J. M. Bauer, Q. Yu, R. H. Liu, C. Devadoss and B.-H. Jo, *Nature*, 2000, **404**, 588.
4. M. Ikeda, T. Tanida, T. Yoshii, K. Kurotani, S. Onogi, K. Urayama and I. Hamachi, *Nat Chem*, 2014, **6**, 511.
5. H. J. Oh, M. K. Joo, Y. S. Sohn and B. Jeong, *Macromolecules*, 2008, **41**, 8204.
6. H. J. Moon, D. Y. Ko, M. H. Park, M. K. Joo and B. Jeong, *Chem. Soc. Rev.*, 2012, **41**, 4860.
7. M. He, J. Li, S. Tan, R. Wang and Y. Zhang, *J. Am. Chem. Soc.*, 2013, **135**, 18718.
8. V. Kozlovskaya, J. Chen, C. Tedjo, X. Liang, J. Campos-Gomez, J. Oh, M. Saeed, C. T. Lungu and E. Kharlampieva, *J. Mater. Chem. B*, 2014, **2**, 2494.
9. J. Li, Y. Gao, Y. Kuang, J. Shi, X. Du, J. Zhou, H. Wang, Z. Yang and B. Xu, *J. Am. Chem. Soc.*, 2013, **135**, 9907.
10. G. Cravotto and P. Cintas, *Chem. Soc. Rev.*, 2009, **38**, 2684.
11. F. Yang, J. Wang, L. Cao, R. Chen, L. Tang and C. Liu, *J. Mater. Chem. B*, 2014, **2**, 295.
12. B. Yan, J.-C. Boyer, D. Habault, N. R. Branda and Y. Zhao, *J. Am. Chem. Soc.*, 2012, **134**, 16558.
13. J. Huang and A. Heise, *Chem. Soc. Rev.*, 2013, **42**, 7373.
14. J. N. Hunt, K. E. Feldman, N. A. Lynd, J. Deek, L. M. Campos, J. M. Spruell, B. M. Hernandez, E. J. Kramer and C. J. Hawker, *Adv. Mater.*, 2011, **23**, 2327.
15. A. Fraix, R. Gref and S. Sortino, *J. Mater. Chem. B*, 2014, **2**, 3443.
16. J. Zhuang, M. R. Gordon, J. Ventura, L. Li and S. Thayumanavan, *Chem. Soc. Rev.*, 2013, **42**, 7421.
17. M. K. Nguyen, C. T. Huynh, G. H. Gao, J. H. Kim, D. P. Huynh, S. Y. Chae, K. C. Lee and D. S. Lee, *Soft Matter*, 2011, **7**, 2994.
18. X.-D. Xu, L. Liang, H. Cheng, X.-H. Wang, F.-G. Jiang, R.-X. Zhuo and X.-Z. Zhang, *J. Mater. Chem.*, 2012, **22**, 18164.
19. K. Ren, C. He, Y. Cheng, G. Li and X. Chen, *Polym. Chem.*, 2014, DOI: 10.1039/C4PY00420E.
20. B. P. Purcell, D. Lobb, M. B. Charati, S. M. Dorsey, R. J. Wade, K. N. Zellars, H. Doviak, S. Pettaway, C. B. Logdon, J. A. Shuman, P. D. Freels, J. H. Gorman Iii, R. C. Gorman, F. G. Spinale and J. A. Burdick, *Nat. Mater.*, 2014, **13**, 653.
21. M. C. Giano, D. J. Pochan and J. P. Schneider, *Biomaterials*, 2011, **32**, 6471.
22. Y. Chen, X.-H. Pang and C.-M. Dong, *Adv. Funct. Mater.*, 2010, **20**, 579.
23. D. J. Adams and P. D. Topham, *Soft Matter*, 2010, **6**, 3707.
24. Y. Kuang and B. Xu, *Angew. Chem. Int. Ed.*, 2013, **52**, 6944.
25. A. Aggeli, M. Bell, N. Boden, J. N. Keen, P. F. Knowles, T. C. B. McLeish, M. Pitkeathly and S. E. Radford, *Nature*, 1997, **386**, 259.
26. V. K. Kotharangannagari, A. Sánchez-Ferrer, J. Ruokolainen and R. Mezzenga, *Macromolecules*, 2012, **45**, 1982.
27. C. Chen, D. Wu, W. Fu and Z. Li, *Biomacromolecules*, 2013, **14**, 2494.
28. A. P. Nowak, V. Breedveld, L. Pakstis, B. Ozbas, D. J. Pine, D. Pochan and T. J. Deming, *Nature*, 2002, **417**, 424.
29. P. D. Thornton, S. M. R. Billah and N. R. Cameron, *Macromol. Rapid Commun.*, 2013, **34**, 257.
30. J. Fan, R. Li, X. He, K. Seetho, F. Zhang, J. Zou and K. L. Wooley, *Polym. Chem.*, 2014, **5**, 3977.
31. J. Sun and H. Schlaad, *Macromolecules*, 2010, **43**, 4445.
32. J. Zou, F. Zhang, Y. Chen, J. E. Raymond, S. Zhang, J. Fan, J. Zhu, A. Li, K. Seetho, X. He, D. J. Pochan and K. L. Wooley, *Soft Matter*, 2013, **9**, 5951.
33. E. Y. Kang, B. Yeon, H. J. Moon and B. Jeong, *Macromolecules*, 2012, **45**, 2007.
34. J. Huang, C. L. Hastings, G. P. Duffy, H. M. Kelly, J. Raeburn, D. J. Adams and A. Heise, *Biomacromolecules*, 2013, **14**, 200.
35. S. Zhang, W. Fu and Z. Li, *Polym. Chem.*, 2014, **5**, 3346.
36. Y. Cheng, C. He, C. Xiao, J. Ding, H. Cui, X. Zhuang and X. Chen, *Biomacromolecules*, 2013, **14**, 468.
37. J. Fan, J. Zou, X. He, F. Zhang, S. Zhang, J. E. Raymond and K. L. Wooley, *Chem. Sci.*, 2014, **5**, 141.
38. A. M. Oelker, S. M. Morey, L. G. Griffith and P. T. Hammond, *Soft Matter*, 2012, **8**, 10887.
39. M. K. Joo, D. Y. Ko, S. J. Jeong, M. H. Park, U. P. Shinde and B. Jeong, *Soft Matter*, 2013, **9**, 8014.
40. C.-U. Lee, L. Lu, J. Chen, J. C. Garno and D. Zhang, *ACS Macro Letters*, 2013, **2**, 436.
41. K.-S. Krannig, A. Doriti and H. Schlaad, *Macromolecules*, 2014, **47**, 2536.
42. T. J. Deming, *Nature*, 1997, **390**, 386.
43. I. Dimitrov and H. Schlaad, *Chem. Commun.*, 2003, 2944.
44. T. Aliferis, H. Iatrou and N. Hadjichristidis, *Biomacromolecules*, 2004, **5**, 1653.
45. H. Lu and J. Cheng, *J. Am. Chem. Soc.*, 2008, **130**, 12562.
46. I. Conejos-Sánchez, A. Duro-Castano, A. Birke, M. Barz and M. J. Vicent, *Polym. Chem.*, 2013, **4**, 3182.
47. J. Zou, J. Fan, X. He, S. Zhang, H. Wang and K. L. Wooley, *Macromolecules*, 2013, **46**, 4223.
48. J. Zou, X. He, J. Fan, J. E. Raymond and K. L. Wooley, *Chem. Eur. J.*, 2014, DOI: 10.1002/chem.201403027.
49. A. Rösler, H.-A. Klok, I. W. Hamley, V. Castelletto and O. O. Mykhaylyk, *Biomacromolecules*, 2003, **4**, 859.
50. T. Miyazawa, Y. Masuda and K. Fukushima, *J. Polym. Sci.*, 1962, **62**, S62.
51. A. Panitch, K. Matsuki, E. J. Cantor, S. J. Cooper, E. D. T. Atkins, M. J. Fournier, T. L. Mason and D. A. Tirrell, *Macromolecules*, 1997, **30**, 42.
52. D. A. Kirschner, C. Abraham and D. J. Selkoe, *Proc. Natl. Acad. Sci. U.S.A.*, 1986, **83**, 503.
53. H. Shao, T. Nguyen, N. C. Romano, D. A. Modarelli and J. R. Parquette, *J. Am. Chem. Soc.*, 2009, **131**, 16374.
54. V. Castelletto, G. Cheng, S. Furzeland, D. Atkins and I. W. Hamley, *Soft Matter*, 2012, **8**, 5434.
55. Y.-A. Lin, Y.-C. Ou, A. G. Cheetham and H. Cui, *Biomacromolecules*, 2014, **15**, 1419.
56. A. Top, C. J. Roberts and K. L. Kiick, *Biomacromolecules*, 2011, **12**, 2184.

Table of contents:

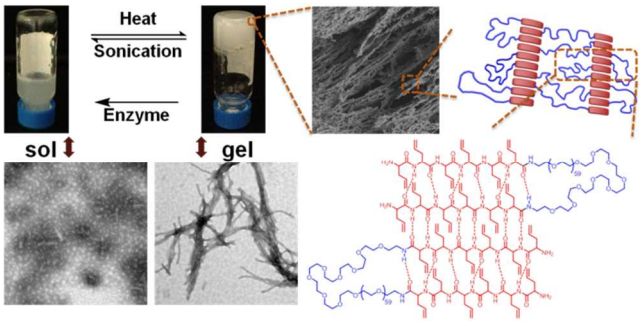

A multi-responsive oligopeptide-based hydrogel system with synthetic feasibility and potential for functionalization provided a platform for intelligent bio-functional and bio-responsive materials.